PCCP

Accepted Manuscript

This article can be cited before page numbers have been issued, to do this please use: L. Yan, Y. Lu and X. Li, *Phys. Chem. Chem. Phys.*, 2016, DOI: 10.1039/C5CP06638G.

ROYAL SOCIETY OF CHEMISTRY

www.rsc.org/pccp

View Article Online
DOI: 10.1039/C5CP06638G

A Density Functional Theory Protocol for the Calculation of Redox Potentials of Copper Complexes

Liuming Yan[a,b,*], Yi Lu[b], Xuejiao Li[a]

a) Department of Chemistry, College of Sciences, Shanghai University, 99 Shangda Road, Shanghai 200444, China

b) Department of Chemistry, University of Illinois at Urbana-Champaign, Urbana, IL 61801, USA

ABSTRACT

A density functional theory (DFT) protocol for the calculation of redox potentials of copper complexes is developed based on 13 model copper complexes. The redox potentials are calculated in terms of Gibbs free energy change of the redox reaction at theory level of CAM-B3LYP/6-31+G(d,p)/SMD, with the overall Gibbs free energy change being partitioned into Gibbs free energy change of gas phase reaction and Gibbs free energy change of solvation. In addition, the calculated Gibbs free energy change of solvation is corrected by a unified correction factor of -0.258 eV as second-layer Gibbs free energy change of solvation and other interactions for each redox reaction. And an empirical Gibbs free energy change of solvation at -0.348 eV is applied to each water molecule if the number of inner-sphere water molecule changes during the redox reaction. Satisfactory agreement between DFT calculated and experimental results are obtained, with a maximum absolute error at 0.197 V, a mean absolute error at 0.114 V and a standard deviation at 0.133 V. Finally, it is concluded that the accurate prediction of redox potentials is dependent on the accurate prediction of geometrical structures as well as on geometrical conservation during redox reaction.

Keywords: redox potential; density functional theory; copper complex; solvation energy

* Corresponding author. Tel.: 8621-66132405, fax: 8621-66132405. E-mail: liuming.yan@shu.edu.cn.

View Article Online
DOI: 10.1039/C5CP06638G

1. Introduction

The tuning of redox potentials of copper proteins represents an important endeavor not only for the understanding of their structural characteristics and functions, but also for the potential engineering applications. After decades of efforts, diverse copper proteins have been developed with fine-tuned redox potentials spanning between -400 and 760 mV, but conserved copper coordination structures [1]. For the better understanding of the relationship between the redox potential and the structural characteristics, the quantum chemistry study especially density functional theory (DFT) calculation of redox potential is of essential important.

Since the DFT calculation of full size copper proteins are beyond reach of the state-of-the-art software and hardware, the study of model copper complexes resembling the coordination structures of copper protein has become a reasonable method for the DFT calculation of redox potential. Recently, the redox potentials of aqueous Ru(III)/Ru(II) solution [2, 3], Ru(III)/Ru(II) complexes bearing bis(N-methyl benzimidazolyl)benzene or -pyridine ligands [4], iron complexes [5], Fischer-type chromium aminocarbene complexes [6], aqueous solutions of fourth-period transition metals [7], group VIII (Fe, Ru, and Os) octahedral complexes [8], $[M(CO)_nL_{6-n}]$ complexes (M = Ru(II)/Ru(III), Os(II)/Os(III), and Tc(II)/Tc(III); L = CN^-, Cl^-, water, CH_3CN, N_2 and CO) [9], artificial water splitting catalyst [10] are successfully calculated. Hughes et al. established a set of empirical parameters for the systematic correcting of errors of DFT spin-splitting energetics and ligand removal enthalpies for transition metal complexes against experimental and CCSD(T)-F12 heats of formation [11, 12], and applied to the accurate evaluation of redox potentials of transition metal complexes and cytochrome P450 [13]. Matsui developed a DFT protocol for the computation of the redox potentials of transition metal complexes with the correction of pseudo-

View Article Online
DOI: 10.1039/C5CP06638G

counterion [14, 15]. Roos studied the effect of non-polar and polar ligands and monovalent cations on the one-electron redox potential of thiyl radical and disulfide bond [16]. Vázquez-Lima et al. modulated the redox potential of a three-coordinated T1 Cu site model based on geometric distortions using DFT calculations [17]. Arumugam et al. reviewed the computation of redox potential of inorganic and organic aqueous complexes, and complexes adsorbed to mineral surfaces [18]. Hoffmann, Jesser, et al. studied the geometrical and optical benchmarking of Cu(II) guanidine-quinoline complexes using various TD-DFT and many-body perturbation theory [19, 20]. Stupka et al. studied the tuning of redox potential by deprotonation of coordinated 1*H*-imidazole in complexes of 2-(1*H*-imidazol-2-yl)pyridine [21]. For detailed information on the accurate DFT calculations of transition metals and transition metal chemistry and biochemistry, the readers are referred to review papers and references here in [22-27].

In spite of these achievements, it has been proved extremely difficult to accurately evaluate redox potentials because the redox potential is the small difference between two very large quantities, the total energies of two oxidation states. In addition, solvation energies, which change significantly during the redox reaction because of the change of charge borne on the metal center, contribute significantly to the total energies. What makes it more complicated is the change in coordination structure for some metal complexes, especially the copper complexes, during oxidation reactions. For complexes without change in coordination structures and with small change in solvation environment, such as the ruthenium complexes, satisfactory results have been achieved by taking account of explicit second solvation layers, however, there lacks successful DFT calculation of redox potentials for copper complexes in literatures.

In this paper, we are going to develop a DFT protocol for the calculation of the redox potentials of copper complexes. First, we will optimize the geometrical structures of both

View Article Online
DOI: 10.1039/C5CP06638G

oxidized and reduced states of 13 model copper complexes in gas phase and solvated state, respectively. And then, we will calculate their Gibbs free energies as well as their Gibbs free energies of solvation. Finally, the DFT protocol for the calculation of redox potential of copper complexes will be concluded and a discussion of the major achievements will be given.

2. Calculation protocol

The Cu(I) and Cu(II) may form coordination compounds with different coordination structures and even with different coordination numbers, and the reduction of a Cu(II) coordination compound may involve inner-sphere rearrangement in aqueous solution,

$$[\mathrm{CuL}(\mathrm{H_2O})_n]^{2+}(\mathrm{aq}) + \mathrm{e}^-(\mathrm{g}) \longrightarrow (n-m)\mathrm{H_2O}(\mathrm{aq}) + [\mathrm{CuL}(\mathrm{H_2O})_m]^{+}(\mathrm{aq}) \quad (1)$$

where $[\mathrm{CuL}(\mathrm{H_2O})_n]^{2+}$ represents the oxidized complex (abbreviated as O), $[\mathrm{CuL}(\mathrm{H_2O})_m]^{+}$ the reduced complex (abbreviated as R), L the multidentate ligand. The standard Gibbs free energy change is evaluated as,

$$\Delta G^{\mathrm{o}}_{\mathrm{O|R}} = \Delta G^{\mathrm{o}}(\mathrm{R(aq)}) + (n-m)\Delta G^{\mathrm{o}}(\mathrm{H_2O(aq)}) - \Delta G^{\mathrm{o}}(\mathrm{O(aq)}) \quad (2)$$

where $\Delta G^{\mathrm{o}}(\mathrm{R(aq)})$, $\Delta G^{\mathrm{o}}(\mathrm{O(aq)})$, and $\Delta G^{\mathrm{o}}(\mathrm{H_2O(aq)})$ are standard Gibbs free energies of the reduced complex, the oxidized complex, and the water molecule in aqueous solution. In order to evaluate the standard Gibbs free energy change $\Delta G^{\mathrm{o}}_{\mathrm{O|R}}$ from gas phase calculations and solvation theory calculations, a Born-Haber cycle is designed (**Fig. 1**), and the Gibbs free energy change is,

$$-\Delta G^{\mathrm{o}}_{\mathrm{O|R}} = \Delta G^{\mathrm{o}}_{\mathrm{II}} + \Delta\Delta G^{\mathrm{o}}_{\mathrm{s}} \quad (3)$$

where the Gibbs free energy change of solvation is,

$$\Delta\Delta G^{\mathrm{o}}_{\mathrm{s}} = \Delta G^{\mathrm{o}}_{\mathrm{s}}(\mathrm{O}) - \Delta G^{\mathrm{o}}_{\mathrm{s}}(\mathrm{R}) - (n-m)\Delta G^{\mathrm{o}}_{\mathrm{s}}(\mathrm{H_2O}) \quad (4)$$

View Article Online
DOI: 10.1039/C5CP06638G

and the Gibbs free energy change for the gas phase oxidation reaction is,

$$\Delta G^{o}_{II} = \Delta G^{o}(\mathrm{O(g)}) - \Delta G^{o}(\mathrm{R(g)}) - (n-m)\Delta G^{o}(\mathrm{H_2O(g)}) \quad (5)$$

The redox potential relative to the standard hydrogen electrode (SHE) is evaluated as the standard Gibbs free energy change subtracting the Gibbs free energy change for the standard hydrogen electrode ΔG^{o}_{SHE} [3],

$$E^{o}_{O|R} = -\frac{1}{F}(\Delta G^{o}_{O|R} - \Delta G^{o}_{SHE}) \quad (6)$$

where F is the Faraday constant, and the widely accepted value of ΔG^{o}_{SHE} is -4.28 eV [28]. The Gibbs free energy of a gas molecule at temperature T is evaluated as,

$$G_T = \varepsilon_{DFT} + \varepsilon_{ZPE} + G_{th} \quad (7)$$

where ε_{DFT}, ε_{ZPE}, and G_{th} are total energy, zero point energy, and thermal correction to the Gibbs free energy at temperature T.

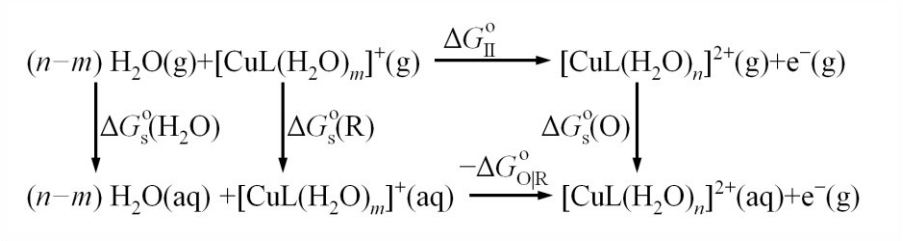

Fig. 1. Born-Haber cycle for the calculation of redox potentials of copper complexes

The complexity in using this procedure to calculate redox potential comes from the fact that the inner-sphere coordination number of the Cu(I)/Cu(II) complexes doesn't always conserve during solvation. On the one hand, it is difficult to make a clear cut between an inner-sphere water molecule and a second-sphere water molecule because the interaction between the

View Article Online
DOI: 10.1039/C5CP06638G

Cu(I)/Cu(II) and the water molecule is weak and the distance between them may change continuously when different ligand, especially when a ligand with large steric repulsion, is involved. On the other hand, the solvation weakens the complexation interaction and blurs further the difference between the first and the second-sphere water molecules. In our calculations, the number of inner-sphere water molecules is determined by a try-and-error procedure: First, the complexes are optimized in gas phase. And then, a solvation model is applied and the complexes are reoptimized. In cases that a water molecule is rejected from the inner-sphere during solvation, the complex will be reoptimized by removing the rejected water molecule both for the gas phase and for the solvated state. From our calculations, it is revealed that this adjustment of inner-sphere water molecule doesn't bring significant difference because the energy difference between the Cu(I)/Cu(II) and the last inner-sphere water molecule and the Cu(I)/Cu(II) and a second-sphere water molecule is insignificance.

Recently, Kepp reviewed the DFT calculations of metal–ligand bonds and spin-crossover in inorganic chemistry, and concluded that molecular geometries are less sensitive to the method and can be modeled quite accurately by most widely used GGA and hybrid functionals, with mean absolute errors of 0.02 Å for bonds and 1 - 2 ° for angles. However, geometries of molecules with very weak bond or significant dispersion interaction, such as the soft Cu-S bond in copper complexes, may subject to larger functional-dependent error and require special attention[29]. Sousa et al. compared the performance of 18 density functionals and 14 basis sets in terms of bond lengths and angles in 50 Cu(II)/Cu(I) complexes, and concluded that the double hybrid GGA and long-range corrected hybrid GGA functionals provide the best description of these copper complexes, and the application of diffuse functions, 6-31+G(d) and 6-31+G(d,p), grants the best geometrical description, while the triple-ζ basis sets do not convey with large

View Article Online
DOI: 10.1039/C5CP06638G

improvement on the geometrical description [23].

In order to evaluate the convergence of the basis sets, the Gibbs free energy change of one redox reaction is calculated in gas phase using four functionals in combination with five basis sets. The redox reaction is between the Cu(I)/Cu(II) complexes with ligand **L1**, bis(1*H*-imidazol-2-yl)-methylamine as shown in **figure 2**, the functionals are CAM-B3LYP, B3PW91, CAM-B3LYP-D3, and ωB97X-D, and the basis sets are 6-31G(d), 6-31G(d,p), 6-31G(2d,p), 6-31+G(d,p), and 6-31+G(2d,p). From these calculations (**figure SI-2**), which are provided in detail as supplementary information, it is concluded that the Gibbs free energy change converges at basis set 6-31+G(d,p); therefore, the 6-31+G(d,p) basis set will be used in all the following calculations.

In addition to the basis set, a suitable combination of functional and solvation model is of essential important since the Gibbs free energy of solvation always outweigh the redox potential of the Cu(II)/Cu(I) couple. Among the many solvation models, the SMD version of universal solvation model, which evaluates the energy of the quantum mechanical charge density of a solute molecule interacting with a continuum description of the solvent, is widely accepted in the calculation of Gibbs free energy of solvation [30]. The choice of functional and solvation model is based on their relative stableness in terms of Gibbs free energy change of the previous redox reaction in aqueous solution. First, the Cu(I)/Cu(II) complexes in aqueous solution are optimized using the four functionals in combination with three solvation models, SMD, IEFPCM, and CPCM. And then, their Gibbs free energies of solvation are evaluated. Finally, the Gibbs free energy change of the redox reaction in aqueous solution is evaluated (also detailed as supplementary information). From **table SI**-4, it is concluded that the CAM-B3LYP density functional is the most stable functional in combination with various solvation models, and the

View Article Online
DOI: 10.1039/C5CP06638G

SMD solvation model is the most stable solvation model in combination with various functionals. Therefore, the CAM-B3LYP density functional in combination with the SMD solvation model is applied throughout this study.

In the following calculations, we are going to optimize the Cu(II)/Cu(I) complexes using the proved density functional and basis set combination of CAM-B3LYP/6-31+G(d,p) in gas phase and the proved density functional, basis set, and solvation model combination of CAM-B3LYP/6-31+G(d,p)/SMD in aqueous solution. All the optimized structures are proved to be local minimum by frequency calculations, and all the calculations are carried out using the GAUSSIAN 09 suite of programs.[31]

3. Results and discussion

3.1 Model ligands

This paper is going to study the redox potential of 13 copper coordination compounds composed of 13 multidentate ligands with sulfur and nitrogen atoms as donors as shown in **figure 2**. The experimental $E^{exp}_{O|R}$ and calculated $E^{calc}_{O|R}$ redox potentials of the copper complexes composed of these multidentate ligands are summarized in **table 1**.

View Article Online
DOI: 10.1039/C5CP06638G

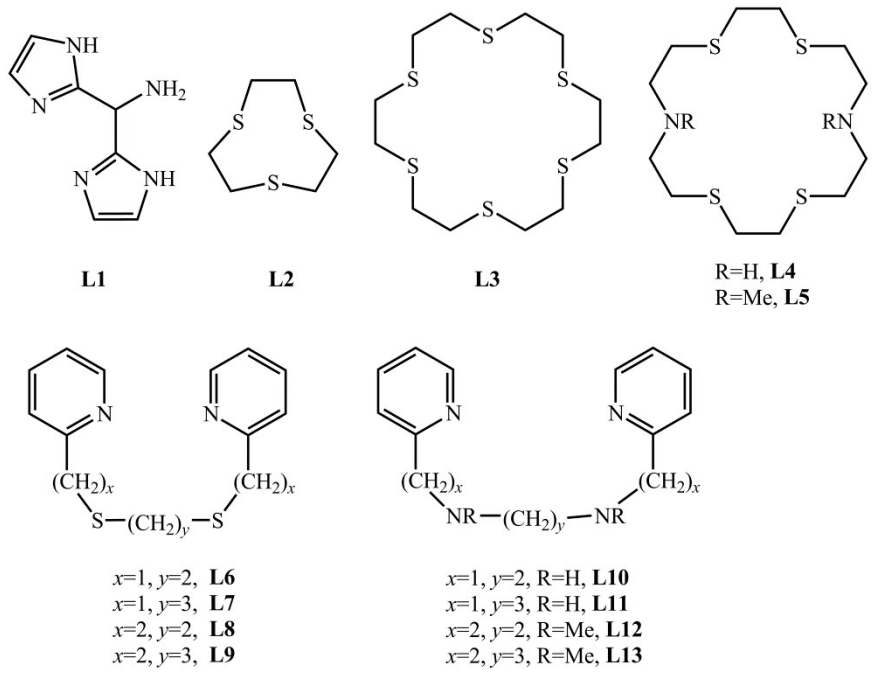

Fig. 2. Model ligands

Table 1. Model ligands and redox potentials of the copper complexes

Ligand	Name of ligand	$E^{exp}_{O\|R}$ (V)	$E^{calc}_{O\|R}$ (V)	ref.
L1	bis(1*H*-imidazol-2-yl)-methylamine	-0.091	0.104	[32]
L2	1,4,7-trithiacyclononane	0.76	0.574	[33]
L3	1,4,7,10,13,16-hexathiacyclooctadecane	0.88	0.861	[34]
L4	1,4,10,13-tetrathia-7,16-diazacyclooctadecane	0.33	0.246	[35]
L5	7,16-dimethyl-1,4,10,13-tetrathia-7,16-diazacyclooctadecane	0.70	0.503	[35, 36]
L6	1,2-bis((pyridin-2-ylmethyl)thio)ethane	0.396	0.303	[37]
L7	1,3-bis((pyridin-2-ylmethyl)thio)propane	0.473	0.575	[37]
L8	1,2-bis((2-(pyridin-2-yl)ethyl)thio)ethane	0.586	0.710	[37]
L9	1,3-bis((2-(pyridin-2-yl)ethyl)thio)propane	0.592	0.654	[37]

View Article Online
DOI: 10.1039/C5CP06638G

L10	N1,N2-bis(pyridin-2-ylmethyl)ethane-1,2-diamine	-0.196	-0.127	[37]
L11	N1,N3-bis(pyridin-2-ylmethyl)propane-1,3-diamine	-0.106	-0.267	[37]
L12	N1,N2-dimethyl-N1,N2-bis(2-(pyridin-2-yl)ethyl)ethane-1,2-diamine	0.099	0.135	[37]
L13	N1,N3-dimethyl-N1,N3-bis(2-(pyridin-2-yl)ethyl)propane-1,3-diamine	0.275	0.425	[37]

3.2 Structures for the copper complexes

The molecular structures of the copper complexes optimized at UCAM-B3LYP/6-31+G(d,p)/SMD level of theory are shown in **figure 3**, and some of their structural parameters are summarized in **table 2.** Here are brief descriptions for the structural characteristics of the copper complexes:

$[Cu(\mathbf{L1})_2]^+$ and $[Cu(\mathbf{L1})_2]^{2+}$: The reduced complex forms an inner-sphere of $[CuN_4]^+$ in a tetrahedral structure with an average Cu–N distance of 2.078 Å. During oxidation, the inner-sphere slightly shrinks to an average Cu–N distance of 2.001 Å, and the dative bonds rotate resulting a slightly twisted square planar structure. Three different conformational isomers are optimized: both $–NH_2$ groups are in axial conformation, both $–NH_2$ groups are in equatorial conformation, either $–NH_2$ groups in axial or equatorial conformation. The axial $–NH_2$ group is slightly stable compared with the equatorial $–NH_2$ group attributing to the release of steric repulsion. The redox potential is evaluated from the most stable conformational isomers of both the copper(II) and the copper(I) complexes.

$[Cu(\mathbf{L2})_2]^+$ and $[Cu(\mathbf{L2})_2]^{2+}$: Each **L2** ligand possesses three sulfur atoms being able to coordinate with the copper atom, and two ligands can form six dative bonds with the copper atom at most. However, the reduced complex forms a tetrahedral structure of $[CuS_4]^+$, and the

View Article Online
DOI: 10.1039/C5CP06638G

oxidized complex forms an axially elongated octahedral structure of $[CuS_6]^{2+}$ with equatorial Cu–S distances at 2.357 to 2.391 Å, and axial Cu–S distances at 2.658 and 2.882 Å. The crystal $[Cu(\mathbf{L2})_2](BF_4)_2 \cdot 2CH_3CN$ shows similar coordination structure with Cu–S distances at 2.419, 2.426, and 2.459 Å without axially elongation [33].

$[Cu\mathbf{L3}]^+$ and $[Cu\mathbf{L3}]^{2+}$: There are two possible configurations for the complex of a cyclic hexadentate ligand in an octahedral structure: mesomeric (meso) in which the two S–S–S linkages each bind facially to the metal center and racemic (rac) in which the two S–S–S portions each bind meridionally to the metal center [36]. From our calculations, it is found that the meso configuration is 0.048 eV lower than the rac configuration for the reduced complex, and the meso conformation is 0.024 eV lower than the rac conformation for the oxidized complex. The reduced complex in meso conformation forms a distorted tetrahedral structure of $[CuS_4]^+$ with four Cu–S bonds slightly varying at 2.306. 2.333, 2.393 and 2.424 Å, and the other two Cu–S distances are at 4.156 and 4.251 Å, while the oxidized complex forms a tetragonally-distorted octahedral structure with four short Cu–S bonds at about 2.406 Å, and two long Cu–S bonds at about 2.772 Å. This inner-sphere change is attributed to the increased attraction between Cu and S during oxidation. The XRD experiments also showed that the oxidized complex has a tetragonally elongated octahedral structure in a meso configuration with four short Cu–S bonds at 2.323 and 2.402 Å, and two long Cu–S bonds at 2.635 Å, slightly shorter than our calculation. And the reduced complex possesses a distorted tetrahedral structure of $[CuS_4]^+$ with Cu–S bonds at 2.245, 2.253, 2.358, and 2.360 Å, being consistent with our calculation [34].

$[Cu\mathbf{L4}]^+$ and $[Cu\mathbf{L4}]^{2+}$: Both complexes form tetragonally compressed octahedral structures of $[CuN_2S_4]$ in rac configuration. For the reduced complex, the rac configuration is 0.146 eV lower than the meso configuration, and the Cu–N distances are at about 2.153 Å, and

View Article Online
DOI: 10.1039/C5CP06638G

Cu–S distances at 2.603 and 2.888 Å for the rac configuration. For the oxidized complex, the rac configuration is 0.490 eV lower than the meso configuration, and the Cu–N distances are at 2.039 and 2.045 Å, and Cu–S distances are at 2.488 to 2.731 Å for the rac configuration. The experiment also showed that the oxidized complex has a tetragonally compressed octahedral structure in a rac configuration with Cu–N bonds at 2.007 and 2.036 Å, and Cu–S bonds at 2.487, 2.528, 2.577, 2.578 Å, being consistent with our calculations [35]. The inner-sphere of the reduced complex could also be regarded as a tetrahedral structure because two of the long Cu–S bonds are elongated to about 2.888 Å, already at marginal distance of the Cu–S coordination interaction.

[Cu**L5**]$^{+}$ and [Cu**L5**]$^{2+}$: The reduced complex forms meso configuration with an inner-sphere of [CuN_2S_2] in distorted tetrahedral structure. The bonded Cu–N distances are at 2.086, 2.088 Å, and two bonded Cu–S distances are at 2.487 to 2.529 Å. The oxidized complex forms a meso configuration in distorted octahedral structure with the Cu–N bonds at 2.118 and 2.135 Å and the Cu–S bonds at 2.432, 2,437, 2.742, and 2.828 Å. The crystal structure of [Cu**L5**]$^{2+}$ is also in distorted octahedral structure with Cu–S bonds at 2.496 Å and Cu–N bonds at 2.191 Å, with the macrocyclic ring adopting the meso configuration, being consistent with our calculations [35, 36].

[Cu**L6**]$^{+}$ and [Cu**L6**(H_2O)]$^{2+}$: The inner-sphere of reduced complex forms distorted tetrahedral structure [CuN_2S_2] with Cu–N distances at 2.014 Å and Cu–S distances at 2.435 Å. When this complex is oxidized, the Cu^{2+} ion attracts an additional water molecule forming a five coordinated inner-sphere of [CuN_2S_2O] in trigonal bipyramidal structure. The two axial Cu–N bonds are at 1.987 Å, and the equatorial Cu-S distances are at 2.403 and 2.443 Å and Cu-O distance is at 2.075 Å. These structural characteristics are consistent with experimental observation [37].

View Article Online
DOI: 10.1039/C5CP06638G

[Cu**L7**(H_2O)]$^+$ and [Cu**L7**(H_2O)]$^{2+}$: The inner-sphere of reduced complex forms distorted tetrahedral structure of [CuN_2SO]. This structure differs from [Cu**L6**]$^+$ where the inner-sphere is [CuN_2S_2], as one of the sulfur atoms is excluded from the inner-sphere attributing to the formation of unbalanced 5-membered ring and 6-membered ring. For the oxidized complex, it forms an inner-sphere of [CuN_2S_2O] in a trigonal bipyramidal structure, similar to that of [Cu**L6**(H_2O)]$^{2+}$.

[Cu**L8**]$^+$ and [Cu**L8**(H_2O)]$^{2+}$, [Cu**L9**]$^+$ and [Cu**L9**(H_2O)]$^{2+}$, [Cu**L10**]$^+$ and [Cu**L10**(H_2O)]$^{2+}$, [Cu**L11**]$^+$ and [Cu**L11**(H_2O)]$^{2+}$, [Cu**L12**]$^+$ and [Cu**L12**(H_2O)]$^{2+}$: These complexes form similar structures to [Cu**L6**]$^+$ and [Cu**L6**(H_2O)]$^{2+}$. The reduced complexes possess distorted tetrahedral structures with an inner-sphere of [CuN_2S_2], and the oxidized complexes form trigonal bipyramidal or distorted square pyramidal structures by attracting of one water molecule as the fifth ligand, also being consistent with experimental observation [37]. In the crystal structure of [Cu**L10**](ClO_4)$_2$, the ligand occupies an equatorial plane and oxygen atoms of perchlorate anions are in the axial position resulting a 4 + 2 coordination compound. This Cu(II)–ligand structure is consistent with our DFT calculations, and the Cu–N distances at 1.980, 1.992, 1.992, and 1.992 Å are only slightly shorter than our results [38]. As a matter of fact, the Cu(II) complexes possess highly variable coordination geometries and may form different types of complexes, however, the distorted square-planar structure is generally conserved[38].

[Cu**L13**]$^+$ and [Cu**L13**]$^{2+}$: Both reduced and oxidized complexes form distorted tetrahedral structure with inner-sphere of [CuN_2S_2]. The lack of water molecule in coordination inner-sphere of the oxidized complex is attributed to the steric repulsion and no water molecule can approach to the center Cu atom.

View Article Online
DOI: 10.1039/C5CP06638G

Table 2 Structural characteristics of the copper complexes

Complex	Structure	Cu–N / Cu–S / Cu–O distances (Å) †
$[Cu(\mathbf{L1})_2]^+$	tetrahedral	2.073, 2.074, 2.081, 2.082
$[Cu(\mathbf{L1})_2]^{2+}$	twisted square planar	1.999, 1.999, 2.002, 2.002
$[Cu(\mathbf{L2})_2]^+$	tetrahedral	2.356, 2.356, 2.394, 2.394, **3.338**, **3.338**
$[Cu(\mathbf{L2})_2]^{2+}$	elongated octahedral	2.357, 2.381, 2.381, 2.391, 2.658, 2.882
$[Cu\mathbf{L3}]^+$	distorted tetrahedral (meso)	2.306, 2.333, 2.393, 2.424, **4.156**, **4.251**
$[Cu\mathbf{L3}]^{2+}$	elongated octahedral (meso)	2.394, 2.406, 2.410, 2.415, 2.757, 2.788
$[Cu\mathbf{L4}]^+$	distorted octahedral (rac)	2.153, 2.154, 2.602, 2.604, 2.888, 2.889
$[Cu\mathbf{L4}]^{2+}$	distorted octahedral (rac)	2.039, 2.045, 2.483, 2.488, 2.665, 2.731
$[Cu\mathbf{L5}]^+$	distorted tetrahedral (meso)	2.086, 2.088, 2.487, 2.529, **4.847**, **4.999**
$[Cu\mathbf{L5}]^{2+}$	distorted octahedral (meso)	2.118, 2.135, 2.432, 2.437, 2.742, 2.828
$[Cu\mathbf{L6}]^+$	distorted tetrahedral	2.014, 2.014, 2.435, 2.435
$[Cu\mathbf{L6}(H_2O)]^{2+}$	trigonal bipyramidal	1.986, 1.987, 2.403, 2.443, 2.075
$[Cu\mathbf{L7}(H_2O)]^{+}$ ‡	distorted tetrahedral	1.980, 2.052, 2.351, **3.557**, 2.493
$[Cu\mathbf{L7}(H_2O)]^{2+}$	trigonal bipyramidal	2.008, 2.085, 2.322, 2.364, 2.231
$[Cu\mathbf{L8}]^+$	distorted tetrahedral	2.027, 2.052, 2.325, 2.425
$[Cu\mathbf{L8}(H_2O)]^{2+}$	trigonal bipyramidal	2.013, 2.030, 2.377, 2.615, 2.065
$[Cu\mathbf{L9}]^+$	distorted tetrahedral	2.027, 2.052, 2.325, 2.425
$[Cu\mathbf{L9}(H_2O)]^{2+}$	trigonal bipyramidal	2.027, 2.205, 2.336, 2.336, 2.101
$[Cu\mathbf{L10}]^+$	distorted tetrahedral	2.000, 2.000, 2.240, 2.240
$[Cu\mathbf{L10}(H_2O)]^{2+}$	distorted square pyramidal	2.002, 2.010, 2.016, 2.020, 2.544
$[Cu\mathbf{L11}]^+$	distorted tetrahedral	2.008, 2.032, 2.157, 2.214
$[Cu\mathbf{L11}(H_2O)]^{2+}$	distorted square pyramidal	2.003, 2.020, 2.040, 2.053, 2.347
$[Cu\mathbf{L12}]^+$	distorted tetrahedral	2.002, 2.030, 2.158, 2.234

View Article Online
DOI: 10.1039/C5CP06638G

[Cu**L12**(H_2O)]$^{2+}$	distorted square pyramidal	2.017, 2.066, 2.081, 2.225, 2.136
[Cu**L13**]$^{+}$	distorted tetrahedral	2.050, 2.058, 2.141, 2.152
[Cu**L13**]$^{2+}$	distorted tetrahedral	2.031, 2.035, 2.061, 2.064

† the bond distances are arranged in order of Cu–N, Cu–S, and Cu–O

‡ *CN* = 4, but it forms $[CuN_2S(H_2O)]^{+}$ instead of $[CuN_2S_2]^{+}$

View Article Online
DOI: 10.1039/C5CP06638G

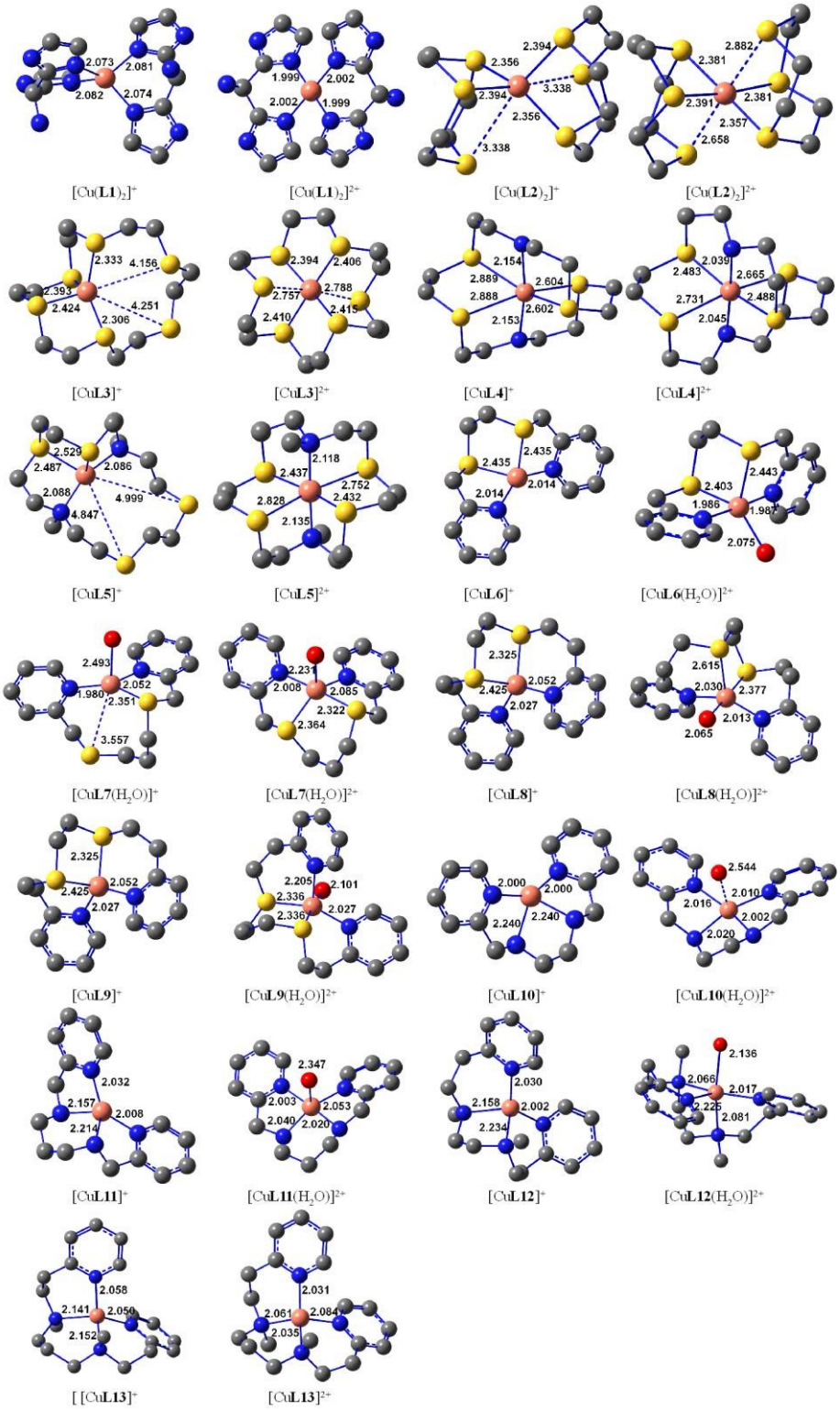

Fig. 3 Structures of the copper complexes, the hydrogen atoms are omitted for clarity and the numbers are bond distance in Å (color code: blue N, yellow S, red O, ochre Cu, grey C).

View Article Online
DOI: 10.1039/C5CP06638G

3.3 Energetics for the copper complexes

Table 3 summarizes the DFT calculated energetic properties for the copper complexes as well as for the corresponding redox reactions. The Gibbs free energy change of gas phase for the redox reaction varies from 8.857 to 9.899 eV, with an average value of 9.404 eV. In solution, the copper complexes are solvated depending on the strength of the electric field in vicinity of the copper complexes. A Cu(II) complex generates a much higher electric field than its corresponding Cu(I) complex, resulting much higher Gibbs free energy of solvation for the Cu(II) complex than its corresponding Cu(I) complex. The average Gibbs free energy of solvation for the Cu(II) complexes is -5.776 eV, compared to an average value of -1.432 eV for the Cu(I) complexes. In the calculation of Gibbs free energy change of solvation, $\Delta\Delta G_s^o$, an empirical Gibbs free energy of solvation at -0.348 eV is used for a water molecule in equation 5 instead of the DFT calculated Gibbs free energy of solvation at -0.171 eV at the same level of theory. The Gibbs free energy change of solvation $\Delta\Delta G_s^o$ varies from -4.154 to -4.883 eV with an average value of -4.505 eV. As a result, the Gibbs free energy change for the redox reaction in solution greatly decreases compared to the Gibbs free energy change of gas phase.

In order to improve the calculation results, numeric corrections are applied to the Gibbs free energy changes of the redox reactions accounting for the contribution from second-layer solvation and other interactions. By comparison the DFT Gibbs free energy changes and the experimental redox potentials, a unified correction factor of -0.258 eV is added to the Gibbs free energy changes of the redox reactions for the copper complexes:

$$\Delta G_{O|R}^c = \Delta G_{O|R}^o - 0.258 \quad (8)$$

View Article Online
DOI: 10.1039/C5CP06638G

where $\Delta G^{c}_{O|R}$ represents the corrected Gibbs free energy changes of the redox reactions.

Table 3 Energetics for the copper complexes and for the redox reactions based on DFT calculations

Ligand	$\Delta G^{o}(O(g))$ (a.u.)	$\Delta G^{o}(R(g))$ (a.u.)	$\Delta G^{o}_{s}(O)$ (eV)	$\Delta G^{o}_{s}(R)$ (eV)	ΔG^{o}_{II} (eV)	$\Delta\Delta G^{o}_{s}$ (eV)	$-\Delta G^{o}_{O\|R}$ (eV)	$-\Delta G^{c}_{O\|R}$ (V)
L1	-2731.07276	-2731.39827	-5.919	-1.704	8.857	-4.215	4.642	4.384
L2	-4500.19389	-4500.54047	-5.868	-1.550	9.431	-4.319	5.112	4.854
L3	-4500.19520	-4500.54873	-5.939	-1.719	9.620	-4.220	5.399	5.141
L4	-3814.47705	-3814.81954	-6.040	-1.504	9.319	-4.535	4.784	4.526
L5	-3892.97496	-3893.31287	-5.786	-1.633	9.195	-4.154	5.041	4.783
L6	-3164.76966	-3165.12481	-5.920	-1.445	9.664	-4.823	4.841	4.583
L7	-3204.03414	-3204.38240	-5.711	-1.347	9.476	-4.364	5.113	4.855
L8	-3243.29958	-3243.66335	-5.654	-1.352	9.899	-4.651	5.248	4.990
L9	-3282.55926	-3282.91577	-5.491	-1.330	9.701	-4.509	5.192	4.934
L10	-2479.04719	-2479.38873	-5.949	-1.414	9.294	-4.883	4.411	4.153
L11	-2518.32409	-2518.65814	-5.805	-1.335	9.090	-4.819	4.271	4.013
L12	-2636.08898	-2636.43476	-5.538	-1.150	9.409	-4.736	4.673	4.415
L13	-2598.95273	-2599.29454	-5.474	-1.136	9.301	-4.338	4.963	4.705

3.4 Redox potentials for the copper complexes

The redox potential with respect to the standard hydrogen electrode is evaluated by subtraction of a value of 4.28 eV from the Gibbs free energy change of the redox reaction as shown in equation 6. The calculated redox potentials, as well as their corresponding experimental values, of the copper complexes are summarized in **table 1**, and their comparisons

View Article Online
DOI: 10.1039/C5CP06638G

are depicted in **figure 4**,

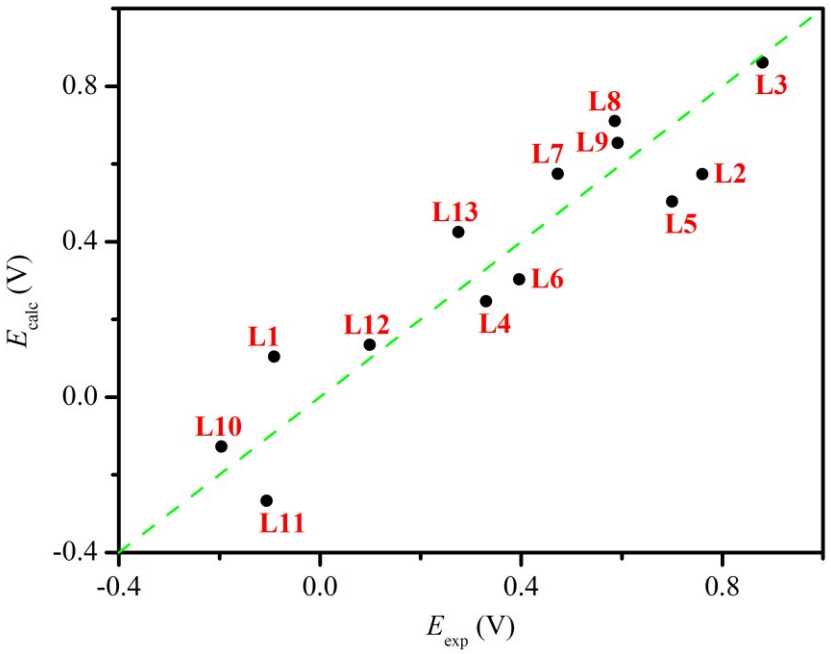

Fig. 4 Comparison of calculated and experimental redox potentials for the copper complexes

Compared with literature calculations, our DFT calculated redox potentials agree satisfactory with the experimental redox potentials. For example, our calculation shows a maximum absolute error at 0.197 V, a mean absolute error at 0.114 V and a standard deviation at 0.133 V for the copper complexes, while the standard deviation between DFT calculated and experimental redox potentials of aqueous Ru^{3+}/Ru^{2+} is about 0.14 V [3]. This is a satisfactory result considering the great structural differences among the copper complexes, and the differences between the reduced and oxidized states of each redox couple. In addition, it is concluded that the calculated value is overestimated when only the first coordination layer is treated explicitly, whereas it is underestimated when the first two hydration layers are considered in the cluster model[3]. In our calculation, only the first coordination layer is explicitly treated,

View Article Online
DOI: 10.1039/C5CP06638G

while the influence from the second coordination layer and other interactions is approximated by a uniform correction factor of -0.258 V. Furthermore, the mean absolute error is 0.112 V for 18 iron complexes, slightly better than our calculation [5]. Therefore, our calculation shows similar error with literature calculations of complexes other than copper complexes.

The calculation error is attributed to the structural change and the interaction from second to the first coordination layer during redox reaction. For example, complex of ligand **L5** possesses the maximum absolute error as its first coordination layer changes from $[CuN_2S_4]^{2+}$ to $[CuN_2S_2]^{+}$ during the reduction reaction. The complexes of $[Cu(\mathbf{L1})_2]^{2+}$ and $[Cu(\mathbf{L2})_2]^{2+}$, which are the only two complexes composed of two ligands, possess large calculation error at 0.195 and -0.185 V as these complexes is more likely to undergo large structural fluctuation than the complexes composed of only one ligand. As a matter of fact, the DFT calculated redox potential is very sensitive to the optimized geometries of the redox couple because their total energies are sensitive to the optimized geometries.

4. Conclusions

A DFT protocol for the calculation of redox potentials of model copper complexes is developed in terms of Gibbs free energy change of the redox reaction. All the Gibbs free energy changes are evaluated at theory level of UCAM-B3LYP/6-31+G(d,p)/SMD, and the overall Gibbs free energy change is partitioned into Gibbs free energy change in gas phase, Gibbs free energy change of solvation, and correction to the Gibbs free energy change from the second-layer solvation and other interactions. The correction to the Gibbs free energy change from the second-layer solvation and other interactions is optimized to -0.258 eV for each redox couple, and the Gibbs free energy change of solvation for each water molecule is optimized to -0.348 eV,

View Article Online
DOI: 10.1039/C5CP06638G

instead of the DFT calculated value of -0.171 eV. This protocol is satisfactory with maximum absolute error at 0.197 V, mean absolute error at 0.114 V and standard deviation at 0.133 V for all the copper complexes.

In addition, the accurate prediction for redox potentials depends greatly on the accurate prediction of the geometrical structures as well as the geometrical conservation during the redox reaction. If the redox couple undergoes large structural change during redox reaction, large calculation error is expected, on the other hand, accurate calculation redox potential can be expected if the structures of the redox couple conserve during redox reaction,

Acknowledgements

The authors thank the financial support from the Chinese National Science Foundation (Nos. 21376147, 21573143), the Innovation Program of Shanghai Municipal Education Commission (13ZZ078), and the 085 Knowledge Innovation Program, and they also acknowledge the High Performance Computing Center of Shanghai University for computing support. One of the authors, Liuming Yan, also thank the financial support from the China Scholarship Council under file number 201406895003 as visiting scholar at University of Illinois at Urbana-Champaign.

References

1. J. Liu, S. Chakraborty, P. Hosseinzadeh, Y. Yu, S. Tian, I. Petrik, A. Bhagi and Y. Lu, *Chem. Rev.*, 2014, **114**, 4366-4469.
2. A. V. Marenich, A. Majumdar, M. Lenz, C. J. Cramer and D. G. Truhlar, *Angew. Chem. Int. Ed.*, 2012, **51**, 12810-12814.

View Article Online
DOI: 10.1039/C5CP06638G

3. P. Jaque, A. V. Marenich, C. J. Cramer and D. G. Truhlar, *J. Phys. Chem. C*, 2007, **111**, 5783-5799.

4. W.-W. Yang, Y.-W. Zhong, S. Yoshikawa, J.-Y. Shao, S. Masaoka, K. Sakai, J. Yao and M.-A. Haga, *Inorg. Chem.*, 2011, **51**, 890-899.

5. H. Kim, J. Park and Y. S. Lee, *J. Comput. Chem.*, 2013, **34**, 2233-2241.

6. H. Kvapilová, I. Hoskovcová, J. Ludvík and S. Záliš, *Organometallics*, 2014, **33**, 4964-4972.

7. M. Uudsemaa and T. Tamm, *J. Phys. Chem. A*, 2003, **107**, 9997-10003.

8. L. Rulíšek, *J. Phys. Chem. C*, 2013, **117**, 16871-16877.

9. J. Moens, F. D. Proft and P. Geerlings, *Phys. Chem. Chem. Phys.*, 2010, **12**, 13174-13181.

10. M. G. Mavros, T. Tsuchimochi, T. Kowalczyk, A. McIsaac, L.-P. Wang and T. V. Voorhis, *Inorg. Chem.*, 2014, **53**, 6386-6397.

11. T. F. Hughes, J. N. Harvey and R. A. Friesner, *Phys. Chem. Chem. Phys.*, 2012, **14**, 7724-7738.

12. T. F. Hughes and R. A. Friesner, *J. Chem. Theory Comput.*, 2011, **7**, 19-32.

13. T. F. Hughes and R. A. Friesner, *J. Chem. Theory Comput.*, 2012, **8**, 442-459.

14. T. Matsui, Y. Kitagawa, Y. Shigeta and M. Okumura, *J. Chem. Theory Comput.*, 2013, **9**, 2974-2980.

15. T. Matsui, Y. Kitagawa, M. Okumura, Y. Shigeta and S. Sakaki, *J. Comput. Chem.*, 2013, **34**, 21-26.

16. G. Roos, F. De Proft and P. Geerlings, *Chem. Eur. J.*, 2013, **19**, 5050-5060.

17. H. Vázquez-Lima, P. Guadarrama and C. Martínez-Anaya, *J. Mol. Model.*, 2012, **18**, 455-466.

View Article Online
DOI: 10.1039/C5CP06638G

18. K. Arumugam and U. Becker, *Minerals*, 2014, **4**, 345-387.

19. A. Hoffmann, M. Rohrmüller, A. Jesser, I. Dos Santos Vieira, W. G. Schmidt and S. Herres-Pawlis, *J. Comput. Chem.*, 2014, **35**, 2146-2161.

20. A. Jesser, M. Rohrmüller, W. G. Schmidt and S. Herres-Pawlis, *J. Comput. Chem.*, 2014, **35**, 1-17.

21. G. Stupka, L. Gremaud and A. F. Williams, *Helv. Chim. Acta*, 2005, **88**, 487-495.

22. C. J. Cramer and D. G. Truhlar, *Phys. Chem. Chem. Phys.*, 2009, **11**, 10757-10816.

23. S. F. Sousa, G. R. P. Pinto, A. J. M. Ribeiro, J. T. S. Coimbra, P. A. Fernandes and M. J. Ramos, *J. Comput. Chem.*, 2013, **34**, 2079-2090.

24. A. C. Tsipis, *RSC Advances*, 2014, **4**, 32504-32529.

25. A. C. Tsipis, *Coord. Chem. Rev.*, 2014, **272**, 1-29.

26. R. J. Deeth, A. Anastasi, C. Diedrich and K. Randell, *Coord. Chem. Rev.*, 2009, **253**, 795-816.

27. M. R. A. Blomberg, T. Borowski, F. Himo, R.-Z. Liao and P. E. M. Siegbahn, *Chem. Rev.*, 2014, **114**, 3601-3658.

28. C. P. Kelly, C. J. Cramer and D. G. Truhlar, *J. Phys. Chem. B*, 2006, **110**, 16066-16081.

29. K. P. Kepp, *Coord. Chem. Rev.*, 2013, **257**, 196-209.

30. A. V. Marenich, C. J. Cramer and D. G. Truhlar, *J. Phys. Chem. B*, 2009, **113**, 6378-6396.

31. M. J. Frisch, G. W. Trucks, H. B. Schlegel, G. E. Scuseria, M. A. Robb, J. R. Cheeseman, G. Scalmani, V. Barone, B. Mennucci, G. A. Petersson, et al., *GAUSSIAN 09, Revision D.02*, 2009.

32. G. Csire, J. Demjén, S. Timári and K. Várnagy, *Polyhedron*, 2013, **61**, 202-212.

33. W. N. Setzer, C. A. Ogle, G. S. Wilson and R. S. Glass, *Inorg. Chem.*, 1983, **22**, 266-271.

View Article Online
DOI: 10.1039/C5CP06638G

34. J. A. R. Hartman and S. R. Cooper, *J. Am. Chem. Soc.*, 1986, **108**, 1202-1208.

35. N. Atkinson, A. J. Blake, M. G. B. Drew, G. Forsyth, A. J. Lavery, G. Reid and M. Schroder, *J. Chem. Soc., Chem. Commun.*, 1989, 984-986.

36. G. Reid and M. Schroder, *Chem. Soc. Rev.*, 1990, **19**, 239-269.

37. D. E. Nikles, M. J. Powers and F. L. Urbach, *Inorg. Chem.*, 1983, **22**, 3210-3217.

38. E. V. Rybak-Akimova, A. Y. Nazarenko, L. Chen, P. W. Krieger, A. M. Herrera, V. V. Tarasov and P. D. Robinson, *Inorg. Chim. Acta*, 2001, **324**, 1-15.